

Kinetic Regulation of the Synthesis of Pentatwinned Gold Nanorods below Room Temperature

Published as part of *The Journal of Physical Chemistry virtual special issue "Marie-Paule Pileni Festschrift"*.

Ana Sánchez-Iglesias,* Kellie Jenkinson, Sara Bals, and Luis M. Liz-Marzán*

Cite This: *J. Phys. Chem. C* 2021, 125, 23937–23944

Read Online

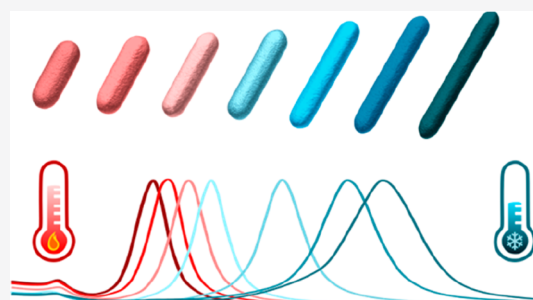
ACCESS |

Metrics & More

Article Recommendations

Supporting Information

ABSTRACT: The synthesis of gold nanorods requires the presence of symmetry-breaking and shape-directing additives, among which bromide ions and quaternary ammonium surfactants have been reported as essential. As a result, hexadecyltrimethylammonium bromide (CTAB) has been selected as the most efficient surfactant to direct anisotropic growth. One of the difficulties arising from this selection is the low solubility of CTAB in water at room temperature, and therefore the seeded growth of gold nanorods is usually performed at 25 °C or above, which has restricted so far the analysis of kinetic effects derived from lower temperatures. We report a systematic study of the synthesis of gold nanorods from pentatwinned seeds using hexadecyltrimethylammonium chloride (CTAC) as the principal surfactant and a low concentration of bromide as shape-directing agent. Under these conditions, the synthesis can be performed at temperatures as low as 8 °C, and the corresponding kinetic effects can be studied, resulting in temperature-controlled aspect ratio tunability.



INTRODUCTION

Gold nanorods (AuNRs) have received significant attraction during the past 20 years because of their potential application in a variety of fields, including plasmon-enhanced spectroscopies,¹ biomedicine,^{2,3} chemical sensing,⁴ photonic and optoelectronic devices,⁵ among others.⁴ Since the seminal reports by Wang et al.,⁶ Murphy et al.,^{7,8} and Nikoobakht and El-Sayed,⁹ the seeded growth of AuNRs in the presence of the cationic surfactant hexadecyltrimethylammonium bromide (CTAB) has been optimized by many other research groups,^{10–17} by introducing either modifications in the synthesis conditions or molecular additives (often cosurfactants) in the growth solution. These modifications showed interesting effects on the growth of gold nanorods, thereby allowing further adjustment of AuNR shape, size, and purity (shape and size monodispersity).

The growth of nanoparticles from seeds usually involves a mild reducing agent and therefore is slower than methods not involving preformed seeds (one-pot nucleation and growth).^{18,19} As a result, a wide variety of shape anisotropy modes can be achieved from seeded-growth approaches. In the paradigmatic case of gold nanorods, as the most representative example of seeded growth, it is reasonable to assume that the reduction kinetics can be further slowed by using lower reaction temperatures, which would further increase anisotropy and, in turn, the aspect ratio of the final nanoparticle product. As obvious as it seems, this hypothesis remains without experimental demonstration. The main reason is that AuNR

synthesis requires the use of a bromide-containing surfactant (CTAB), which is insoluble in water (it precipitates out) at temperatures below 25 °C, making it difficult to realize synthesis experiments below this temperature. The use of alternative surfactants, such as the bromide-free hexadecyltrimethylammonium chloride (CTAC, soluble above 5 °C), is usually ruled out because chloride counterions have a low adsorption energy on Au surfaces and are inefficient with regard to symmetry breaking in gold nanorods.^{20,21} To mitigate the problem of using CTAB at low temperatures, researchers have explored alternative mechanisms that modulate the reduction kinetics, including the addition of silver^{22,23} and halide ions,^{24–26} or the variation of seed concentration and pH.^{10,27–29} Although all of these additives do alter the kinetics of gold reduction, in turn affecting the final aspect ratio, they also complicate the final composition. On the other hand, although temperature is the most straightforward parameter to tune reaction kinetics, it remains barely explored.^{30,31} It should be noted that most of the work reported on the use of additives has been performed by using

Received: August 17, 2021

Revised: September 30, 2021

Published: October 22, 2021



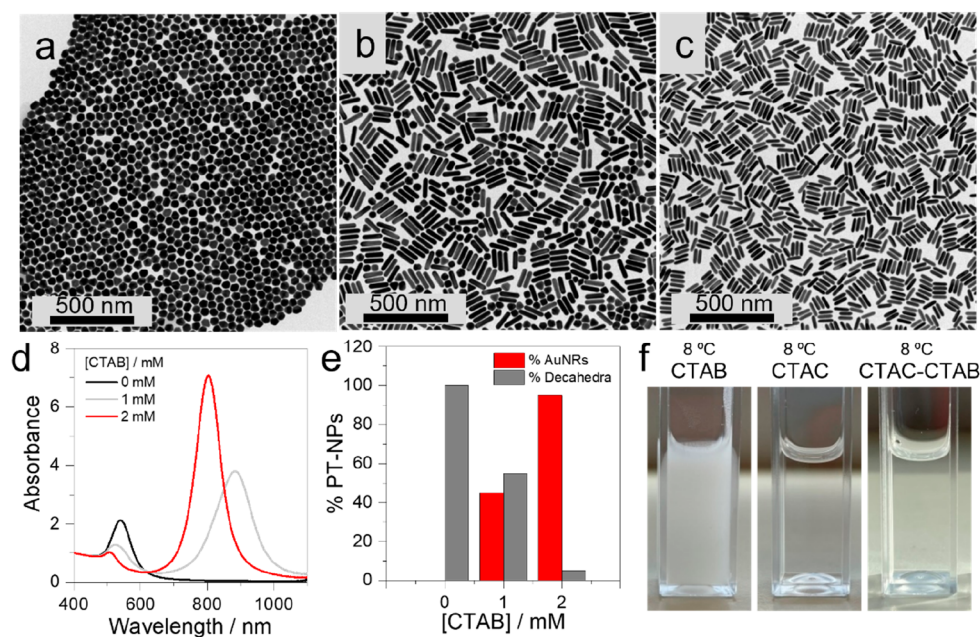


Figure 1. Effect of CTAB concentration on the yield of pentatwinned gold nanorods at constant CTAC concentration (100 mM). (a–c) TEM images of gold nanoparticles obtained in the absence of CTAB (a), in the presence of CTAB 1 mM (b), and in the presence of CTAB 2 mM (c). (d) UV–vis–NIR spectra (normalized at 400 nm) of gold nanoparticles synthesized in the absence of CTAB and in binary mixtures of CTAC and CTAB with different CTAB concentrations. (e) Quantification of isotropic and anisotropic nanoparticles obtained in the presence of different CTAB concentrations. (f) Photographs of aqueous solutions of pure CTAB, pure CTAC, and a CTAC–CTAB mixture stored at 8 °C for 60 min.

single crystalline seeds, in turn resulting in monocrystalline AuNRs with octahedral cross section, containing an unknown amount of silver, which is also required during the synthesis.³² On the contrary, additive-free nanorods are usually grown from pentatwinned (decahedral) seeds, so that the 5-fold twinning in the seeds is preserved in the final nanorods as well.³³

We have recently reported a method for the high-yield seeded growth of pentatwinned gold nanorods (PT-AuNRs) with high monodispersity and tunability of both length and width, and thus anisotropy, by optimizing the formation of pentatwinned nanoparticle seeds.³⁴ The significant increase in the proportion of pentatwinned decahedra in the seed solution allowed us to achieve a highly efficient growth of PT-AuNRs with no need for any additives, including Ag^+ ions. We report herein a modification of this optimization protocol, based on the use of CTAC as the primary surfactant and CTAB as a minority additive to induce symmetry breaking. Under these conditions (low bromide concentration), temperature can be used to finely modulate the reduction kinetics of gold nanorod growth. Our results confirm that slower reduction kinetics—at lower temperatures—lead to a gradual increase in the aspect ratio, such that the longitudinal localized surface plasmon resonance (LSPR) band position can be tailored, from 721 up to 1250 nm, as temperature is lowered from 40 to 8 °C, while keeping all other experimental parameters constant. By using this optimized protocol, we can obtain highly monodisperse PT-AuNRs, with aspect ratios ranging from 2.8 to 7.3, through modulation of a single parameter, temperature.

RESULTS AND DISCUSSION

Efficient, high-yield preparation of pentatwinned gold nanoparticles in general (nanorods, nanopyramids, and nanodecahedra) requires optimization of the synthesis of seeds with 5-fold twinning.³⁴ When using optimized seeds, nanoparticle

size can be finely tuned, e.g., by varying the concentration of seeds in the growth solution and by using ascorbic acid (AA) as a mild reducing agent. As mentioned above, the growth of isotropic seeds into highly anisotropic nanorods requires the use of CTAB because bromide (Br^-) ions preferentially adsorb onto {100} facets on the sides of the nanocrystal, leading to favored addition of gold atoms onto {111} facets.²¹ Bromide enhances the adsorption of CTA^+ on gold surfaces due to its higher affinity compared to chloride, so that a facet-selective adsorption of bromide should lead to a facet-selective adsorption of CTA^+ .^{35,36} Additionally, the coordination of Br^- and CTA^+ with gold ions may also slow down their reduction kinetics and favor anisotropic growth.³⁷

Therefore, an important question is: what is the minimum concentration of CTAB needed to induce anisotropic growth? Growing nanoparticles at 20 °C in pure CTAC (temperature commonly used for PT-AuNR synthesis) leads to isotropic nanoparticles, in this case mainly decahedra (Figure 1a,d). Conversely, when the growth solution contains a concentration of CTAB close to its critical micellar concentration (cmc) \sim 1 mM, a mixture of isotropic and anisotropic nanoparticles is obtained (Figure 1b,d). By further increasing CTAB concentration up to 2 mM, the formation of nanorods is strongly favored, as confirmed by transmission electron microscopy (TEM) (Figure 1c) and UV–vis–NIR spectroscopy (Figure 1d). The pentatwinned structure of the obtained nanorods was confirmed by atomic resolution high angle annular dark field scanning transmission electron microscopy (HAADF-STEM), both in 2D and in 3D, as shown in Figure 2, Figure S1, and Figure S2. Quantification of the amount of anisotropic nanoparticles in each sample indicates that 100% isotropic nanoparticles are obtained in the absence of CTAB, whereas near its cmc the percentage of anisotropic nanoparticles goes up to 45%, and an increased CTAB

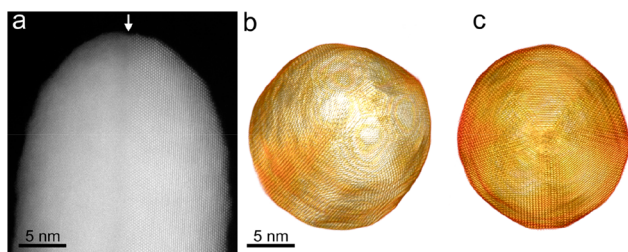


Figure 2. (a) Atomic resolution HAADF-STEM image of a pentatwinned Au nanorod tip to highlight the location of one of the twin boundaries (indicated by a white arrow) and surface faceting. (b, c) 3D visualization of a HAADF-STEM tomography reconstruction along different directions, showing surface faceting and 5-fold symmetry in 3D.

concentration of 2 mM leads to almost exclusive growth of nanorods (95%) (Figure 1e). These results confirm that bromide is responsible for symmetry breaking, while the role of CTAC is related to slowing down the rate of gold precursor reduction and stabilizing nanoparticles against aggregation.³⁶

To further confirm that bromide is critical to induce anisotropic growth, we performed the PT-AuNR synthesis in a growth solution of CTAC (100 mM), containing sodium bromide (NaBr) instead of CTAB, with a final bromide concentration of 2 mM. As expected, PT-AuNRs were also obtained in the presence of bromide from NaBr (Figure S3). Notwithstanding, we preferred to maintain the use of CTAB as the symmetry breaking agent to avoid an unnecessary increase in ionic strength. To show that the selected binary surfactant mixture (CTAC: 100 mM; CTAB: 2 mM) allows us to work at low temperature, we studied the effect of temperature on

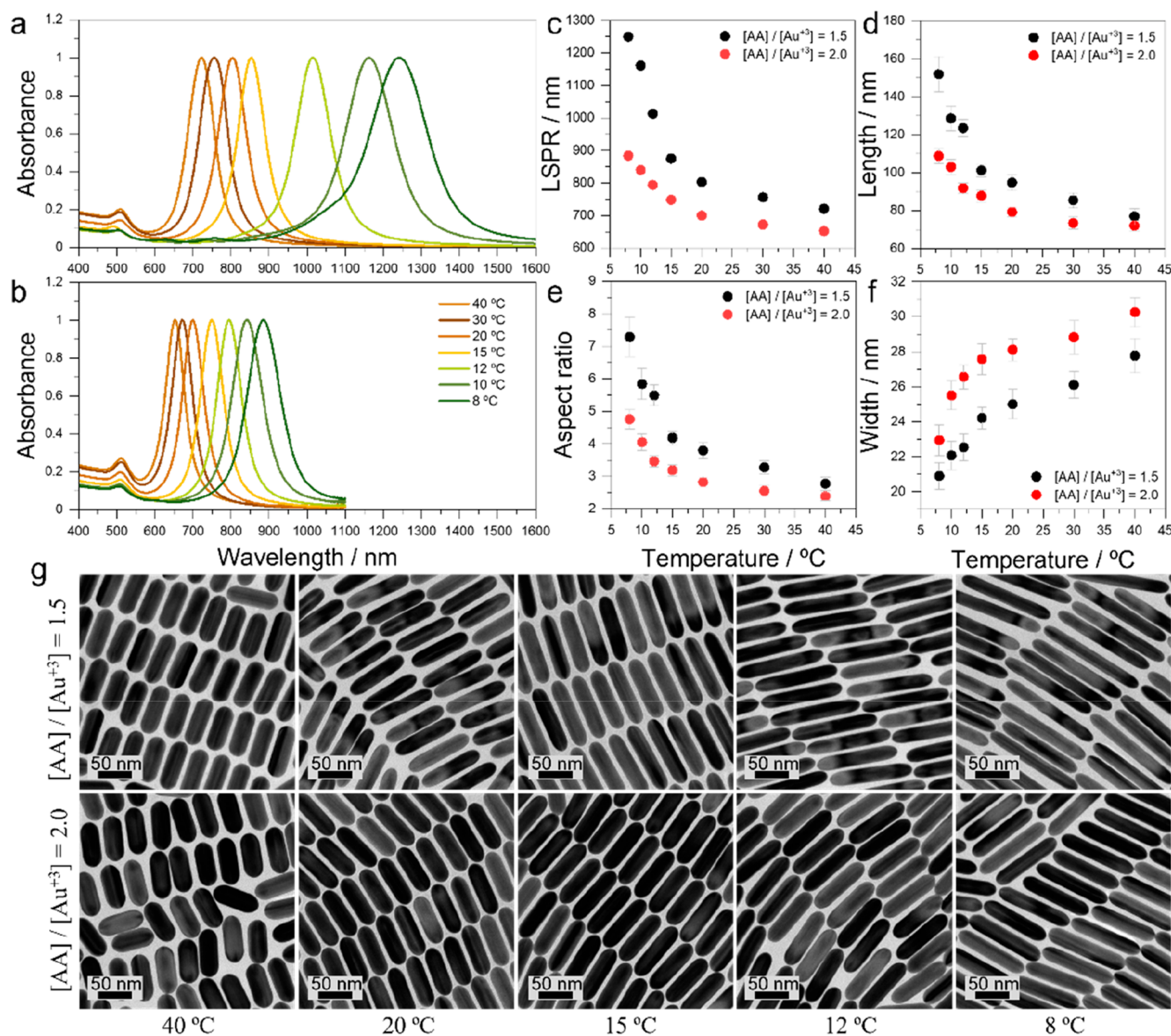


Figure 3. Temperature effect on the dimensions and optical response of PT-AuNRs, obtained with the same AA:Au³⁺ and Au³⁺:Au⁰ molar ratios: (a, b) UV-vis-NIR spectra of gold nanorods grown at different temperatures with AA:Au³⁺ molar ratios of 1.5 (a) and 2.0 (b). (c–f) Variation of various parameters as a function of synthesis temperature, for AA:Au³⁺ = 1.5 (black dots) and 2.0 (red dots): longitudinal LSPR maximum (c), PT-AuNR length (d), aspect ratio (e), and width (f). (g) Representative TEM images of PT-AuNRs obtained at different temperatures for AA:Au³⁺ = 1.5 (upper panel) and 2.0 (lower panel). Further details are provided in Tables S1 and S2 and in Figures S5–S8.

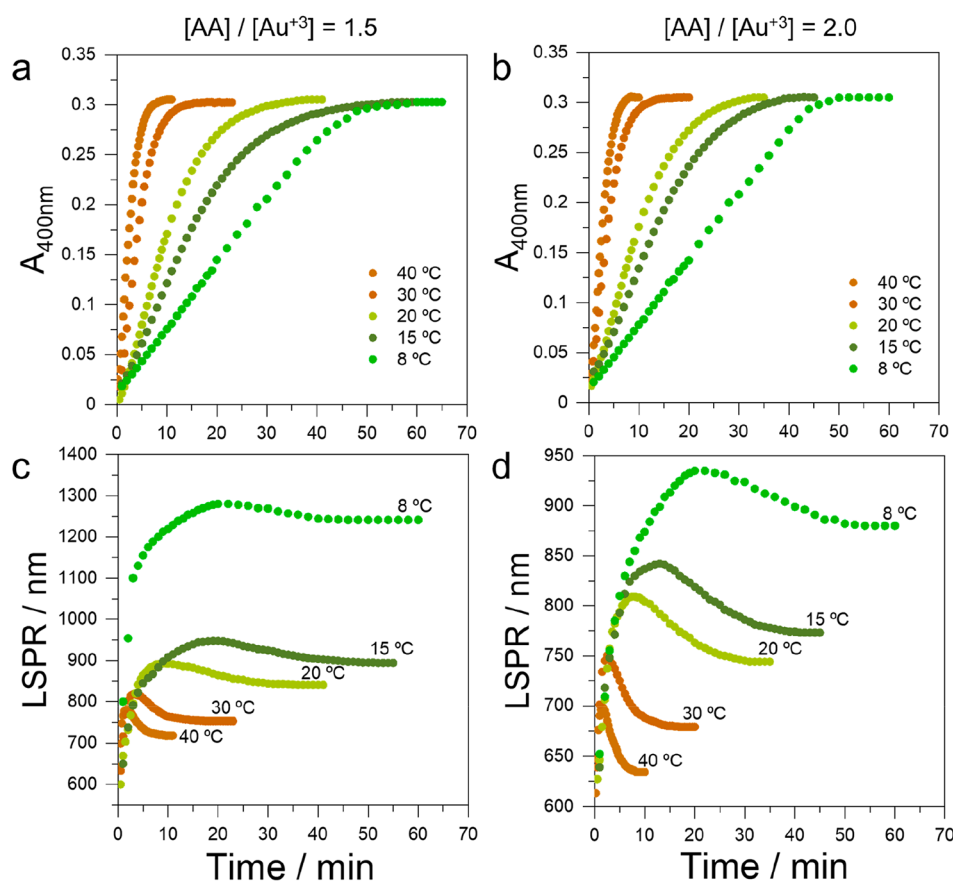


Figure 4. Kinetic study of the growth of gold nanorods at different temperatures, for different $\text{Au}^{3+}:\text{Au}^0$ molar ratios: 1.5 (a, c) and 2.0 (b, d). (a, b) Time traces of the absorbance at 400 nm for different temperatures, as labeled. (c, d) Time traces of the longitudinal LSPR maximum during the growth of gold nanorods at different temperatures, as labeled.

surfactant crystallization from aqueous solution. It is known that CTAB (100 mM) has a solubility threshold of 27 °C, and we indeed observed crystallization at temperatures below 25 °C (Figure 1f and Figure S4a). On the contrary, CTAC (100 mM) can be cooled to 8 °C with no signs of crystallization (Figure 1f and Figure S4b), while the aqueous surfactant mixture (CTAC: 100 mM; CTAB: 2 mM) remains transparent at 8 °C, but crystallization is observed at 5 °C (Figure 1f and Figure S4c).^{38,39}

Therefore, we set 8 °C as the lower temperature limit during our study of the effect of temperature on PT-AuNR growth, and we ran syntheses at different temperatures ranging from 40 to 8 °C (see Figure 3 and Tables S1 and S2), while keeping $\text{AA}:\text{Au}^{3+} = 1.5$ and $\text{Au}^{3+}:\text{Au}^0(\text{seed}) = 133$ molar ratios constant. Highly monodisperse PT-AuNRs were obtained at all temperatures, featuring longitudinal LSPRs that span a wide wavelength range, from 721 to 1250 nm (Figure 3a,c). In turn, the aspect ratio of the obtained PT-AuNRs could be tailored between 2.8 ± 0.2 and 7.3 ± 0.6 (length range from 77 ± 4 to 152 ± 9 nm, width range from 28 ± 1 to 21 ± 1 nm) (Figure 3d–g, Table S1; see histograms and additional TEM images in Figures S5 and S7). Interestingly, when the $\text{AA}:\text{Au}^{3+}$ molar ratio was increased to 2.0, while keeping other experimental parameters constant, we observed a narrower wavelength range for the longitudinal LSPR band, from 652 to 884 nm, when temperature was varied, again between 40 and 8 °C (Figure 3b,c). The aspect ratio of the obtained PT-AuNRs correspondingly varied in a narrower range, between $2.4 \pm$

0.1 and 4.8 ± 0.3 (length from 72 ± 3 to 109 ± 4 nm, width from 30 ± 1 to 23 ± 1 nm) (Figure 3d–g and Table S2; see histograms and additional TEM images in Figures S6 and S8). TEM characterization (Figure 3g and Figures S7 and S8) indeed confirmed that for $\text{AA}:\text{Au}^{3+} = 1.5$ the obtained PT-AuNRs were longer and thinner (higher aspect ratio) as the synthesis temperature was decreased from 40 to 8 °C, compared to those obtained for a higher $\text{AA}:\text{Au}^{3+}$ molar ratio of 2.0. Therefore, it is also confirmed that syntheses at lower temperatures lead to PT-AuNRs with increased aspect ratios, from 2.8 ± 0.2 to 7.3 ± 0.6 for $\text{AA}:\text{Au}^{3+} = 1.5$ and from 2.4 ± 0.1 to 4.8 ± 0.3 for $\text{AA}:\text{Au}^{3+} = 2.0$ (Figure 3e); i.e., a wider variation in aspect ratio was obtained when using a lower $\text{AA}:\text{Au}^{3+}$ molar ratio (1.5).

We propose that the effect of temperature over the aspect ratio of gold nanorods is due to a change in the reaction rates involved in nanorod growth. Therefore, we performed kinetic studies by monitoring the LSPR position and the absorbance at 400 nm (as an indication of Au^0 concentration¹⁶) at different temperatures, for both $\text{AA}:\text{Au}^{3+}$ molar ratios (1.5 and 2.0), keeping all other parameters constant (Figure 4, Tables S1 and S2). It should be noted that in all cases the reduction of gold precursor is fully completed, and the absorbance at 400 nm reaches a maximum value of 0.3 in all kinetic experiments (Figure 4a,b). The most important observation from these experiments was that the rate of gold precursor reduction was significantly slower as temperature was decreased. Gold salt reduction was completed in ca. 10 min at 40 °C, whereas at 8

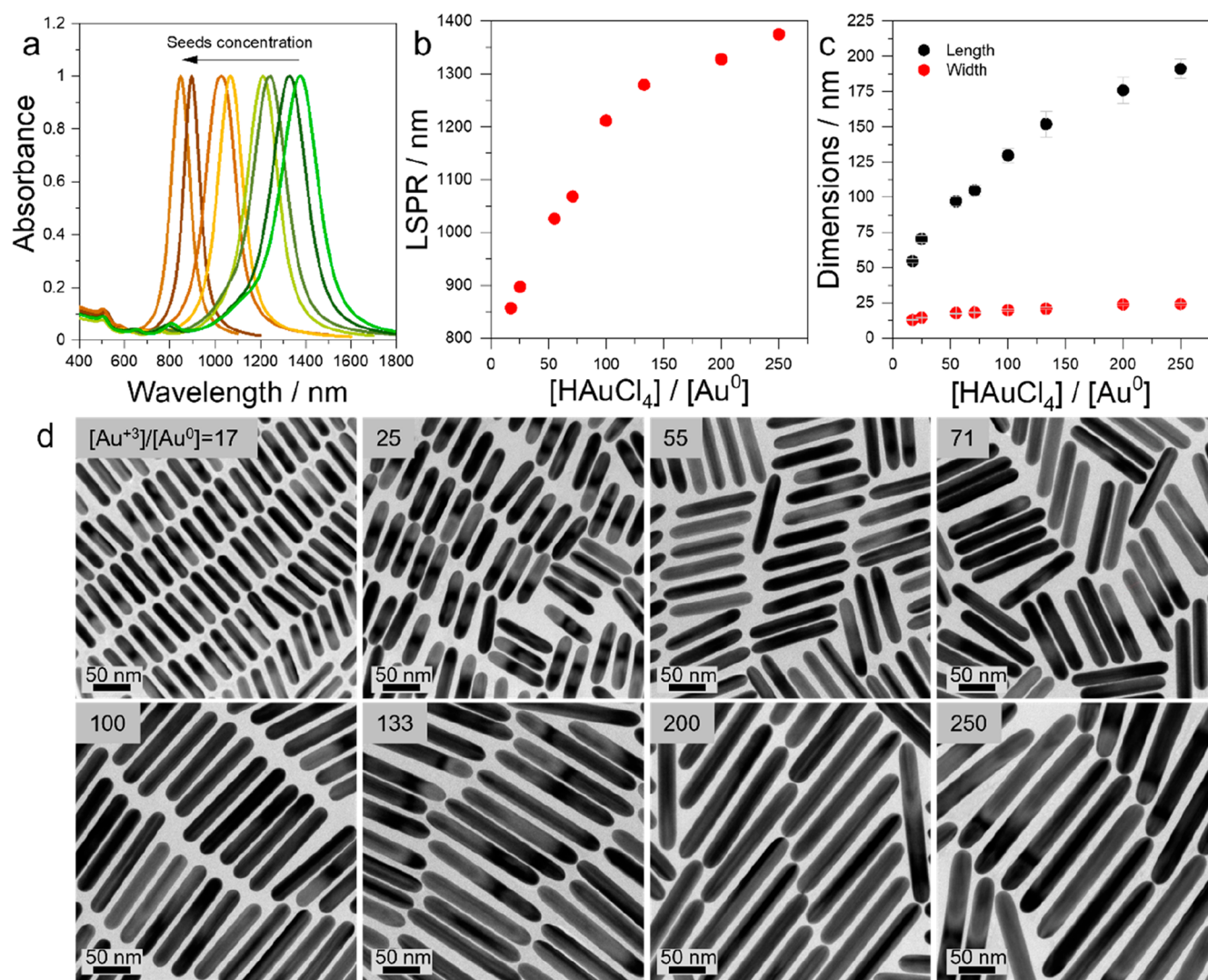


Figure 5. Influence of seed concentration on the growth of pentatwinned gold nanorods at 8 °C for different $\text{Au}^{3+}:\text{Au}^0$ molar ratios, from 17 to 250, keeping all other experimental parameters constant. (a) UV–vis–NIR spectra of PT-AuNRs prepared with different seed concentrations. (b) Dependence of the longitudinal LSPR band wavelength as a function of $\text{Au}^{3+}:\text{Au}^0$ molar ratio. (c) Average dimensions of PT-AuNRs obtained with different $\text{Au}^{3+}:\text{Au}^0$ molar ratios. (d) Representative TEM images of PT-AuNRs prepared with different $\text{Au}^{3+}:\text{Au}^0$ molar ratios, keeping constant the concentration of gold precursor. Further details are provided in Table S3 and Figures S9 and S10.

°C the complete reaction was only achieved after 50 min (Figure 4a,b). The rate of gold reduction (measured as the increase of absorbance at 400 nm) for $\text{AA}:\text{Au}^{3+} = 1.5$ was found to be slower than that for a molar ratio of 2.0, as expected for a decrease in the reaction rate when a lower concentration of reducing agent was used.

We also studied the changes in LSPR position as a function of time, for different temperatures and concentration ratios (Figure 4c,d). In all cases, the longitudinal LSPR displayed an initial red-shift for several minutes of reduction but then gradually blue-shifted until reduction of gold precursor was completed. The extent of such blue-shifts was more pronounced for the higher $\text{AA}:\text{Au}^{3+}$ molar ratio of 2.0. These observations confirm our initial hypothesis; i.e., a slower growth kinetics is obtained by decreasing reaction temperature, leading to an increase in the aspect ratio of the final gold nanorods. The observed LSPR shifts also seem to indicate variations of both length and width over time, which are different for different compositions and temperatures.

As a usual parameter to tune aspect ratio in gold nanorod synthesis, we additionally studied the influence of gold seed concentration, and the obtained results are summarized in Figure 5. We synthesized gold nanorods by varying the $\text{Au}^{3+}:\text{Au}^0$ molar ratio (the ratio between added gold precursor and seeds) at a low temperature of 8 °C and an $\text{AA}:\text{Au}^{3+}$ molar ratio of 1.5 (see details in Table S3). Regardless of seed concentration, highly monodisperse PT-AuNRs were obtained (Figure 5d), with longitudinal LSPR bands spanning a wide wavelength range, from 857 to 1375 nm, when the $\text{Au}^{3+}:\text{Au}^0$ molar ratio was varied from 17 to 250, respectively (Figure 5a,b). The aspect ratio of the obtained nanorods ranged accordingly between 4.2 ± 0.2 and 7.9 ± 0.6 (length from 55 ± 1 to 191 ± 7 nm, width from 13 ± 1 to 24 ± 1 nm) (Figure 5c and Table S3; see histograms and additional TEM images in Figures S9 and S10). It should also be noted that the growth of gold nanorods below room temperature can be performed by using twinned seeds with an average diameter of 6 nm,³⁴ whereas the use of standard 1 nm seeds leads to the formation

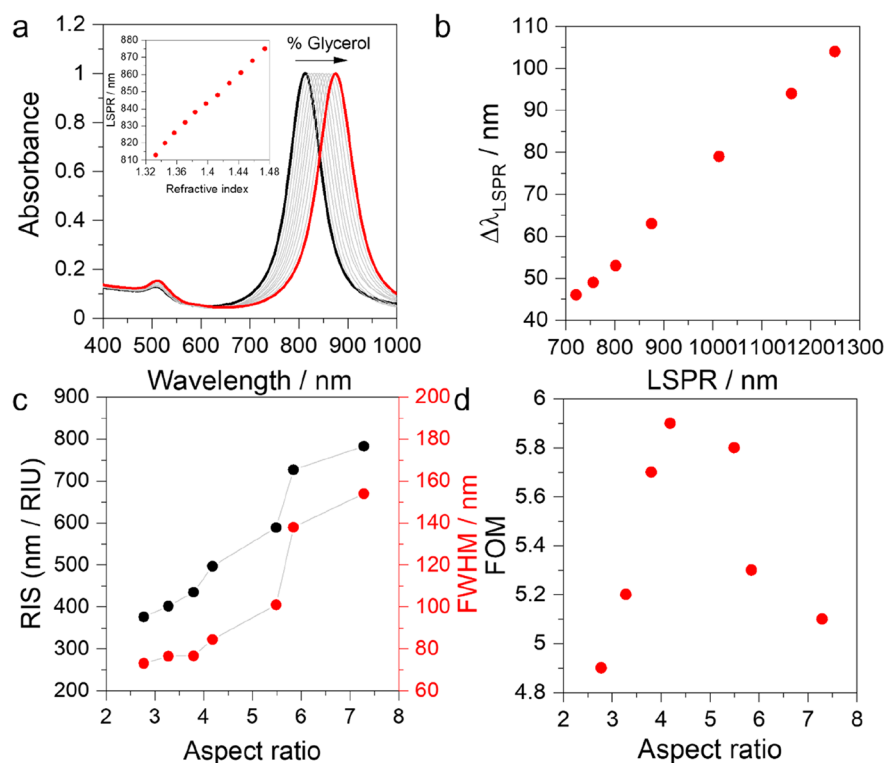


Figure 6. Optical sensitivity of pentatwinned gold nanorods with different aspect ratios. (a) UV–vis–NIR spectra of nanorods with an aspect ratio of 4.2 ± 0.2 , dispersed in water–glycerol mixtures of varying volume fractions (0–100% in glycerol). (b) Maximum plasmon shift ($\Delta\lambda_{\text{LSPR}}$) as a function of the initial longitudinal LSPR band position. (c) RIS and FWHM for PT-AuNRs of different aspect ratios. (d) Dependence of FOM with the aspect ratio of PT-AuNRs. Further details are provided in Table S4.

of isotropic nanoparticles at 20 °C and only a small fraction of nanorods at 8 °C (Figure S11).

As an example of the potential applications of these high-quality PT-AuNRs, we performed a systematic study of the refractive index sensing properties and figures of merit (FOM) of gold nanorods with different aspect ratios (Figure 6). The plasmon resonance of gold nanoparticles is known to depend on particle shape, size, composition, monodispersity, and the refractive index of the surrounding medium.⁴⁰ As a result, plasmonic nanoparticles can be used for sensing of environmental changes, their performance being mainly determined by the so-called refractive index sensitivity (RIS), defined as the magnitude of the LSPR shift per refractive index unit (RIU), and the figure of merit (FOM),⁴¹ determined by the ratio between the refractive index sensitivity and the full width at half-maximum of the LSPR band (FWHM). The LSPR bands in UV–vis–NIR spectra of nanoparticle dispersions red-shift as the refractive index of the surrounding medium is increased. We thus dispersed PT-AuNRs of different aspect ratios (Table S1) in water–glycerol mixtures (0–100% in glycerol), which display a linear variation of refractive index as a function of the volume fraction, as shown in Figure S12.^{42,43} When gold nanorods of different aspect ratios were dispersed in water–glycerol mixtures with increasing glycerol content, the LSPR was found to red-shift for all samples (Figure 6a and Figure S13) as a result of the gradual increase in medium refractive index. Interestingly, the LSPR position displayed a linear dependence with the medium refractive index (Figure 6a, inset, and Figure S14). Additionally, we observed that the plasmon shift ($\Delta\lambda_{\text{LSPR}}$) is also linearly dependent on the initial LSPR

position, meaning that larger shifts were obtained for PT-AuNRs with higher aspect ratios (Figure 6b).

Additional observations can be made from the registered RIS and FWHM for PT-AuNRs with different aspect ratios (Figure 6c and Table S4). The RIS values were found to increase from 376 to 783 nm/RIU and the FWHM from 76 to 154 nm for nanorods with increasing aspect ratios between 2.8 ± 0.2 and 7.3 ± 0.6 , respectively. Whereas both RIS and FWHM follow a similar positive trend as a function of aspect ratio (Figure 6c), the calculated FOM, i.e., RIS/FWHM, features a volcano-like shape with a maximum at 875 nm, which corresponds to an aspect ratio of 4.2 ± 0.2 (Figure 6c,d). Such a nonlinear behavior of the FOM can be explained by a more pronounced contribution of the FWHM in the final FOM value, which is related to the progressive LSPR band broadening as aspect ratio increases.⁴⁴ It should be noted that the FOM values reported here are higher than those previously reported for gold nanorods, which is indicative of the high quality of the samples.⁴²

CONCLUSIONS

We have demonstrated in this work that binary surfactant mixtures of CTAC and CTAB can be used to largely reduce the concentration of bromide during the synthesis of pentatwinned gold nanorods, which in turn offers the possibility to work at unusually low temperatures, even below room temperature. Highly monodisperse nanorods were obtained for various temperatures between 40 and 8 °C, which resulted in a fine modulation of the longitudinal surface plasmon resonance, from 721 to 1250 nm. We clearly showed that the variation in the final dimensions of the

obtained nanorods is due to kinetic effects, as the growth rate displays a significant dependence with reaction temperature. Although we showed an initial study of the nanocrystal growth mechanism, further studies will be possible by expanding the toolbox of reaction parameters. The high quality of the obtained nanorods was also demonstrated through a high refractive index sensitivity, yielding record-high figures of merit.

■ ASSOCIATED CONTENT

SI Supporting Information

The Supporting Information is available free of charge at <https://pubs.acs.org/doi/10.1021/acs.jpcc.1c07284>.

Materials and methods; additional TEM and HAADF-STEM images; selected electron tomography reconstructions; effect of temperature on surfactant crystallization; tables with experimental conditions; size histograms; additional analysis of refractive index sensitivity (PDF)

■ AUTHOR INFORMATION

Corresponding Authors

Ana Sánchez-Iglesias – CIC biomaGUNE, Basque Research and Technology Alliance (BRTA), 20014 Donostia-San Sebastián, Spain; Centro de Investigación Biomédica en Red de Biotecnología, Biomateriales y Nanomedicina (CIBER-BBN), 20014 Donostia-San Sebastián, Spain;
Email: asanchez@cicbiomagune.es

Luis M. Liz-Marzán – CIC biomaGUNE, Basque Research and Technology Alliance (BRTA), 20014 Donostia-San Sebastián, Spain; Centro de Investigación Biomédica en Red de Biotecnología, Biomateriales y Nanomedicina (CIBER-BBN), 20014 Donostia-San Sebastián, Spain; Ikerbasque, Basque Foundation for Science, 48009 Bilbao, Spain;
Email: llizmarzan@cicbiomagune.es

Authors

Kellie Jenkinson – EMAT and NANOLab Center of Excellence, University of Antwerp, 2020 Antwerp, Belgium

Sara Bals – EMAT and NANOLab Center of Excellence, University of Antwerp, 2020 Antwerp, Belgium;

orcid.org/0000-0002-4249-8017

Complete contact information is available at: <https://pubs.acs.org/doi/10.1021/acs.jpcc.1c07284>

Notes

The authors declare no competing financial interest.

■ ACKNOWLEDGMENTS

This project has received funding from the European Union's Horizon 2020 research and innovation program under Grant Agreement No. 861950, project POSEIDON; Grant No. 731019, EUSMI; and ERC Consolidator Grant 815128, REALNANO. This work was performed under the Maria de Maeztu Units of Excellence Program from the Spanish State Research Agency (Grant No. MDM-2017-0720). The authors thank Dr. Marek Grzelczak for useful discussions during this project.

■ REFERENCES

(1) Langer, J.; Jimenez de Aberasturi, D.; Aizpurua, J.; Alvarez-Puebla, R. A.; Auguie, B.; Baumberg, J. J.; Bazan, G. C.; Bell, S. E. J.

Boisen, A.; Brolo, A. G.; et al. Present and Future of Surface-Enhanced Raman Scattering. *ACS Nano* **2020**, *14*, 28–117.

(2) Dreaden, E. C.; Alkilany, A. M.; Huang, X.; Murphy, C. J.; El-Sayed, M. A. The Golden Age: Gold Nanoparticles for Biomedicine. *Chem. Soc. Rev.* **2012**, *41*, 2740–2779.

(3) Cobley, C. M.; Chen, J.; Cho, E. C.; Wang, L. V.; Xia, Y. Gold Nanostructures: A Class of Multifunctional Materials for Biomedical Applications. *Chem. Soc. Rev.* **2011**, *40*, 44–56.

(4) Kabashin, A. V.; Evans, P.; Pastkovsky, S.; Hendren, W.; Wurtz, G. A.; Atkinson, R.; Pollard, R.; Podolskiy, V. A.; Zayats, A. V. Plasmonic Nanorod Metamaterials for Biosensing. *Nat. Mater.* **2009**, *8*, 867–871.

(5) Knight, M. W.; Sobhani, H.; Nordlander, P.; Halas, N. J. Photodetection with Active Optical Antennas. *Science* **2011**, *332*, 702–704.

(6) Yu Chang, S.-S.; Lee, C.-L.; Wang, C. R. C. Gold Nanorods: Electrochemical Synthesis and Optical Properties. *J. Phys. Chem. B* **1997**, *101*, 6661–6664.

(7) Jana, N. R.; Gearheart, L.; Murphy, C. J. Seed-Mediated Growth Approach for Shape-Controlled Synthesis of Spheroidal and Rod-like Gold Nanoparticles Using a Surfactant Template. *Adv. Mater.* **2001**, *13*, 1389–1393.

(8) Jana, N. R.; Gearheart, L.; Murphy, C. J. Wet Chemical Synthesis of High Aspect Ratio Cylindrical Gold Nanorods. *J. Phys. Chem. B* **2001**, *105*, 4065–4067.

(9) Nikoobakht, B.; El-Sayed, M. A. Preparation and Growth Mechanism of Gold Nanorods (NRs) Using Seed-Mediated Growth Method. *Chem. Mater.* **2003**, *15*, 1957–1962.

(10) Busbee, B. D.; Obare, S. O.; Murphy, C. J. An Improved Synthesis of High-Aspect-Ratio Gold Nanorods. *Adv. Mater.* **2003**, *15*, 414–416.

(11) Pérez-Juste, J.; Liz-Marzán, L. M.; Carnie, S.; Chan, D. Y. C.; Mulvaney, P. Electric-Field-Directed Growth of Gold Nanorods in Aqueous Surfactant Solutions. *Adv. Funct. Mater.* **2004**, *14*, 571–579.

(12) Wu, H.-Y.; Chu, H.-C.; Kuo, T.-J.; Kuo, C.-L.; Huang, M. H. Seed-Mediated Synthesis of High Aspect Ratio Gold Nanorods with Nitric Acid. *Chem. Mater.* **2005**, *17*, 6447–6451.

(13) Ye, X.; Jin, L.; Caglayan, H.; Chen, J.; Xing, G.; Zheng, C.; Doan-Nguyen, V.; Kang, Y.; Engheta, N.; Kagan, C. R.; et al. Improved Size-Tunable Synthesis of Monodisperse Gold Nanorods through the Use of Aromatic Additives. *ACS Nano* **2012**, *6*, 2804–2817.

(14) Ye, X.; Zheng, C.; Chen, J.; Gao, Y.; Murray, C. B. Using Binary Surfactant Mixtures To Simultaneously Improve the Dimensional Tunability and Monodispersity in the Seeded Growth of Gold Nanorods. *Nano Lett.* **2013**, *13*, 765–771.

(15) Ye, X.; Gao, Y.; Chen, J.; Reifsnnyder, D. C.; Zheng, C.; Murray, C. B. Seeded Growth of Monodisperse Gold Nanorods Using Bromide-Free Surfactant Mixtures. *Nano Lett.* **2013**, *13*, 2163–2171.

(16) Scarabelli, L.; Grzelczak, M.; Liz-Marzán, L. M. Tuning Gold Nanorod Synthesis through Prereduction with Salicylic Acid. *Chem. Mater.* **2013**, *25*, 4232–4238.

(17) González-Rubio, G.; Kumar, V.; Llombart, P.; Díaz-Núñez, P.; Bladt, E.; Altantzis, T.; Bals, S.; Peña-Rodríguez, O.; Noya, E. G.; MacDowell, L. G.; et al. Disconnecting Symmetry Breaking from Seeded Growth for the Reproducible Synthesis of High Quality Gold Nanorods. *ACS Nano* **2019**, *13*, 4424–4435.

(18) Pérez-Juste, J.; Pastoriza-Santos, N.; Liz-Marzán, L. M.; Mulvaney, P. Gold Nanorods: Synthesis, Characterization and Applications. *Coord. Chem. Rev.* **2005**, *249*, 1870–1901.

(19) Lee, J.; Yang, J.; Kwon, S. G.; Hyeon, T. Nonclassical Nucleation and Growth of Inorganic Nanoparticles. *Nat. Rev. Mater.* **2016**, *1*, 1–16.

(20) Sau, T. K.; Murphy, C. J. Role of Ions in the Colloidal Synthesis of Gold Nanowires. *Philos. Mag.* **2007**, *87*, 2143–2158.

(21) Almora-Barrios, N.; Novell-Leruth, G.; Whiting, P.; Liz-Marzán, L. M.; López, N. Theoretical Description of the Role of Halides, Silver, and Surfactants on the Structure of Gold Nanorods. *Nano Lett.* **2014**, *14*, 871–875.

- (22) Kou, X.; Zhang, S.; Tsung, C.-K.; Yang, Z.; Yeung, M. H.; Stucky, G. D.; Sun, L.; Wang, J.; Yan, C. One-Step Synthesis of Large-Aspect-Ratio Single-Crystalline Gold Nanorods by Using CTPAB and CTBAB Surfactants. *Chem. - Eur. J.* **2007**, *13*, 2929–2936.
- (23) Tong, W.; Walsh, M. J.; Mulvaney, P.; Etheridge, J.; Funston, A. M. Control of Symmetry Breaking Size and Aspect Ratio in Gold Nanorods: Underlying Role of Silver Nitrate. *J. Phys. Chem. C* **2017**, *121*, 3549–3559.
- (24) Smith, D. K.; Miller, N. R.; Korgel, B. A. Iodide in CTAB Prevents Gold Nanorod Formation. *Langmuir* **2009**, *25*, 9518–9524.
- (25) DuChene, J. S.; Niu, W.; Abendroth, J. M.; Sun, Q.; Zhao, W.; Huo, F.; Wei, W. D. Halide Anions as Shape-Directing Agents for Obtaining High-Quality Anisotropic Gold Nanostructures. *Chem. Mater.* **2013**, *25*, 1392–1399.
- (26) Lohse, S. E.; Burrows, N. D.; Scarabelli, L.; Liz-Marzán, L. M.; Murphy, C. J. Anisotropic Noble Metal Nanocrystal Growth: The Role of Halides. *Chem. Mater.* **2014**, *26*, 34–43.
- (27) Wei, Q.; Ji, J.; Shen, J. PH Controlled Synthesis of High Aspect-Ratio Gold Nanorods. *J. Nanosci. Nanotechnol.* **2008**, *8*, 5708–5714.
- (28) Kim, F.; Sohn, K.; Wu, J.; Huang, J. Chemical Synthesis of Gold Nanowires in Acidic Solutions. *J. Am. Chem. Soc.* **2008**, *130*, 14442–14443.
- (29) Liu, M.; Guyot-Sionnest, P. Mechanism of Silver(I)-Assisted Growth of Gold Nanorods and Bipyramids. *J. Phys. Chem. B* **2005**, *109*, 22192–22200.
- (30) Sharma, V.; Park, K.; Srinivasarao, M. Colloidal Dispersion of Gold Nanorods: Historical Background, Optical Properties, Seed-Mediated Synthesis, Shape Separation and Self-Assembly. *Mater. Sci. Eng., R* **2009**, *65*, 1–38.
- (31) Liu, X.; Yao, J.; Luo, J.; Duan, X.; Yao, Y.; Liu, T. Effect of Growth Temperature on Tailoring the Size and Aspect Ratio of Gold Nanorods. *Langmuir* **2017**, *33*, 7479–7485.
- (32) Goris, B.; Bals, S.; Van den Broek, W.; Carbó-Argibay, E.; Gómez-Graña, S.; Liz-Marzán, L. M.; Van Tendeloo, G. Atomic-Scale Determination of Surface Facets in Gold Nanorods. *Nat. Mater.* **2012**, *11*, 930–935.
- (33) Johnson, C. J.; Dujardin, E.; Davis, S. A.; Murphy, C. J.; Mann, S. Growth and Form of Gold Nanorods Prepared by Seed-Mediated, Surfactant-Directed Synthesis. *J. Mater. Chem.* **2002**, *12*, 1765–1770.
- (34) Sánchez-Iglesias, A.; Winckelmans, N.; Altantzis, T.; Bals, S.; Grzelczak, M.; Liz-Marzán, L. M. High-Yield Seeded Growth of Monodisperse Pentatwinned Gold Nanoparticles through Thermally Induced Seed Twinning. *J. Am. Chem. Soc.* **2017**, *139*, 107–110.
- (35) Garg, N.; Scholl, C.; Mohanty, A.; Jin, R. The Role of Bromide Ions in Seeding Growth of Au Nanorods. *Langmuir* **2010**, *26*, 10271–10276.
- (36) Brown, M.; Wiley, B. J. Bromide Causes Facet-Selective Atomic Addition in Gold Nanorod Syntheses. *Chem. Mater.* **2020**, *32*, 6410–6415.
- (37) Langille, M. R.; Personick, M. L.; Zhang, J.; Mirkin, C. A. Defining Rules for the Shape Evolution of Gold Nanoparticles. *J. Am. Chem. Soc.* **2012**, *134*, 14542–14554.
- (38) Chen, Z.; Greaves, T. L.; Fong, C.; Caruso, R. A.; Drummond, C. J. Lyotropic Liquid Crystalline Phase Behaviour in Amphiphile–Protic Ionic Liquid Systems. *Phys. Chem. Chem. Phys.* **2012**, *14*, 3825–3836.
- (39) Henriques Do Aido, T. M.; Alcantara, M. R.; Felipe, O., Jr.; Galvão Pereira, A. M.; Vanin, J. A. Inducer Chemical Nature and the Helical Twist Sense of Cholesteric Lyotropic Mesophases. *Mol. Cryst. Liq. Cryst.* **1991**, *195*, 45–54.
- (40) Liz-Marzán, L. M. Tailoring Surface Plasmons through the Morphology and Assembly of Metal Nanoparticles. *Langmuir* **2006**, *22*, 32–41.
- (41) Mayer, K. M.; Hafner, J. H. Localized Surface Plasmon Resonance Sensors. *Chem. Rev.* **2011**, *111*, 3828–3857.
- (42) Chen, H.; Kou, X.; Yang, Z.; Ni, W.; Wang, J. Shape- and Size-Dependent Refractive Index Sensitivity of Gold Nanoparticles. *Langmuir* **2008**, *24*, 5233–5237.
- (43) Khan, A. U.; Zhao, S.; Liu, G. Key Parameter Controlling the Sensitivity of Plasmonic Metal Nanoparticles: Aspect Ratio. *J. Phys. Chem. C* **2016**, *120*, 19353–19364.
- (44) Otte, M. A.; Sepúlveda, B.; Ni, W.; Juste, J. P.; Liz-Marzán, L. M.; Lechuga, L. M. Identification of the Optimal Spectral Region for Plasmonic and Nanoplasmonic Sensing. *ACS Nano* **2010**, *4*, 349–357.